The Influence of Friction Stir Processing on Microstructure and Properties of a Cast Nickel Aluminum Bronze Material

K. Oh-ishi, A.M. Cuevas, D.L. Swisher and T.R. McNelley

Center for Materials Science, Department of Mechanical Engineering
Naval Post Graduate School, Monterey, California 93943-5146 USA

Abstract

Cast nickel-aluminum bronze (NAB) is specified for many marine applications due to its excellent corrosion resistance. Improved mechanical properties may be attainable using friction stir processing (FSP) to achieve localized microstructure modification in cast material, and convert an as-cast microstructure to a wrought condition in the absence of macroscopic shape change. In effect, FSP provides a means of surface hardening of castings. The complex physical metallurgy of cast NAB material will be reviewed and the effect of FSP on microstructure of an as-cast NAB material will be described.

Introduction

NAB materials are copper-based alloys that are widely used to produce cast components for marine applications. In addition to excellent corrosion resistance, as-cast NABs exhibit good fracture toughness combined with moderate strength; low coefficients of friction and good wear characteristics; non-sparking behavior; high damping capacity; and good fatigue resistance [1]. Many cast components produced in NAB involve thick sections and the slow cooling rates contribute to coarse microstructures and reduced physical and mechanical properties [2]. In many applications NAB castings are not heat treatable and so it would be desirable to have alternative methods available to selective strengthen the surface layers of cast components. This may be achieved by FSP. Friction between a rotating tool and the surface of the material results in a 'stirring' action that, in turn, produces adiabatic heating and local softening. The tool rotation results in very large deformations in the softened regions, and thus microstructure refinement and homogenization leading, in turn, to improved strength and ductility [3-5]. FSP may also result in closure of porosity and redistribution of inclusions thus conferring improved corrosion resistance.

NAB Alloy Constitution. Copper-aluminum alloys containing more that 9.4 wt. % Al solidify as a single-phase bcc β; under slow-cooling conditions, fcc α gradually forms from the β until the remaining β transforms to $\alpha + \gamma$ in a eutectoid reaction at about 570ºC [6]. The γ phase corrodes preferentially due to its high Al content and its presence is thus deleterious [7,8]. The addition of nickel and iron to copper-aluminum alloys extends the α phase field while effectively suppressing γ phase formation [7,9,10]. The Ni and Fe additions have been found to considerably increase NAB mechanical properties through the formation, from both the α and the β, of complex intermetallic κ phases. Thus, NAB is a copper-base quaternary of composition as listed in Table 1.

Table 1. Composition (wt. %) of UNS C95800 NAB Material [11]

Element	Cu	Al	Ni	Fe	Mn	Si	Pb
min-max	Min 79.0	8.5-9.5	4.0-5.0	3.5-4.5	0.8-1.5	max 0.10	max 0.03
nominal	81	9	5	4	1	-	-

Many investigators have described the constitution and transformation characteristics of as-cast NAB materials [7,8,12-20]. A cast NAB alloy solidifies as a single-phase β solid solution (Fig. 1a) although cooling through the liquid + solid region will result in a non-equilibrium distribution of the Al. The sequence of transformations during equilibrium cooling is illustrated in Fig. 1b [8]. The alloy remains fully β upon cooling to about 1000ºC. Below this temperature α phase precipitates from the β with a Widmanstätten morphology, followed by the nucleation of globular κ, which is nominally Fe_3Al, in the β. This phase is apparent in the micrograph of an as-cast NAB in Fig. 1c and is often termed $κ_{ii}$. (In Cu-Al-Ni-Fe alloys containing ≥ 5 wt. % Fe, an Fe_3Al phase forms with a dendritic morphology, which is usually termed $κ_i$ [15,17].) At about 850ºC, the solubility of Fe in the α is exceeded and fine κ precipitates begin to form; these fine precipitates are also nominally Fe_3Al and are usually termed $κ_{iv}$. Finally, at about 580ºC a nickel-rich κ phase, $κ_{iii}$, forms from β by a eutectoid reaction giving lamellar α + $κ_{iii}$. Proeutectoid $κ_{iii}$ may exhibit a globular morphology.

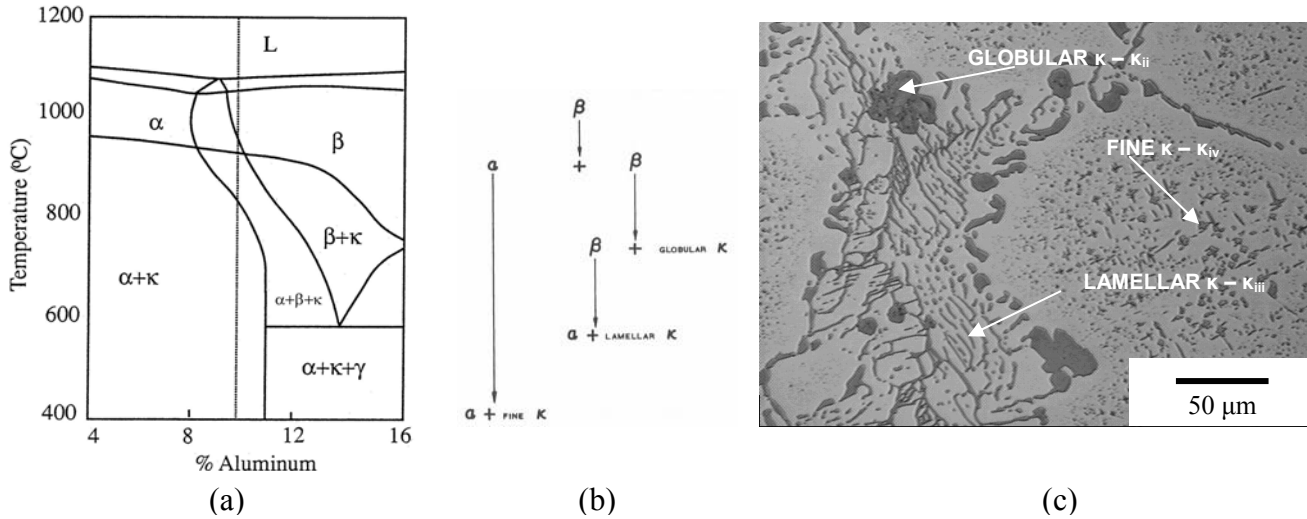(a)   (b)   (c)

Figure 1. (a) The Cu-Al-5Ni-5Fe phase diagram [9,10] and (b) the sequence of transformations for equilibrium cooling of a Cu-9Al-5Ni-5Fe alloy [8]; (c) optical micrograh of as-cast NAB (etched).

The α phase is an fcc equilibrium terminal solid solution with a lattice parameter a = 3.64 Å [15]. The Fe_3Al phases ($κ_i$, $κ_{ii}$ and $κ_{iv}$) have a DO_3 structure; the lattice parameter of $κ_{ii}$ is 5.71 Å while that of $κ_{iv}$ is 5.77 Å [15,17,19]. The NiAl ($κ_{iii}$) phase exhibits a B_2 structure with a lattice parameter of 2.88 Å [15,17,19]. Thus, fully ordered Fe_3Al ($κ_i$, $κ_{ii}$ and $κ_{iv}$) and NiAl ($κ_{iii}$) phases will have inter-atom spacings that differ by less than one percent.

Friction Stir Processing. FSP is an adaptation of friction stir welding (FSW), which was developed at The Welding Institute [21]. In FSP, a cylindrical, wear-resistant tool consisting of a smaller diameter pin with a concentric, larger diameter shoulder is rotated and forced into the surface of a single piece of material. The tool penetrates until the shoulder comes into contact with the work piece surface. The tool is then traversed along a path on the surface of the work piece in single- or multi-pass processes. The shoulder acts to contain upward metal flow caused by pin insertion and metal flow in the work piece involves vertical (parallel to the tool axis) as well as horizontal (in the plane of tool rotation) components. Both FSW and FSP involve large deformations and severe strain, strain rate and temperature gradients. Investigation of microstructure and microtexture during FSW of aluminum alloys has revealed fine, equiaxed, and dynamically recrystallized grains within the weld nugget. It has also been proposed that microstructure development is dominated by slip and dynamic continuous recrystallization wherein

subgrain boundaries accumulate dislocations and increase in disorientation. Shear textures and texture gradients were also been reported [21-23].

Experimental

As-cast NAB material of composition given in Table 2 was examined.

Table 2. Composition (wt. %) of NAB Material

Cu	Al	Ni	Fe	Mn	Zn	Si	Sn	P	Pb
81.2	9.39	4.29	3.67	1.20	0.14	0.05	0.02	0.009	<0.005

FSP was accomplished at the Rockwell Scientific Company, Thousand Oaks, CA using a tool having a shoulder diameter of 23.8 mm and pin depth of 7.95 mm [24]. The pin was also 7.95 mm in depth but tapered and machined with a spiral groove. The material in the present study was processed with a tool rotation rate of 800 rpm and traverse rate of ~152 mm m^{-1} (6 in m^{-1}) [24].

Optical microscopy included standard sample preparation methods. Samples were etched in a two-step process involving, first, immersion for 1 – 2 s in a solution of 40% ammonia – 20% hydrogen peroxide, followed by immersion for 1 s in a solution of 40% phosphoric acid – 10% hydrogen peroxide. Samples were examined using of bright-field illumination in a JENAPHOT 2000 equipped with a digital imaging system. Orientation imaging microscopy (OIM) was conducted with a TOPCON SM-510 scanning electron microscope using a tungsten filament. Transmission electron microscopy (TEM) used a TOPCON 002B operated at 200 kV. Thin foils were prepared using a 33% Nitric acid – 67% Ethanol solution cooled initially to -25ºC.

Results and Discussion

A schematic diagram representing FSP is shown in Fig. 2a while a montage of optical micrographs shows as-cast base metal and the thermo-mechanically affected zone (TMAZ) of the NAB material after FSP (Fig. 2b). The TMAZ is about 20 mm wide and 5 – 6 mm in depth. The boundary between the TMAZ and base metal is sharp on the advancing side and directly under the tool but it is indistinct on the retreating side. Distortion of the base metal grains is evident everywhere along the TMAZ / base metal boundary although the
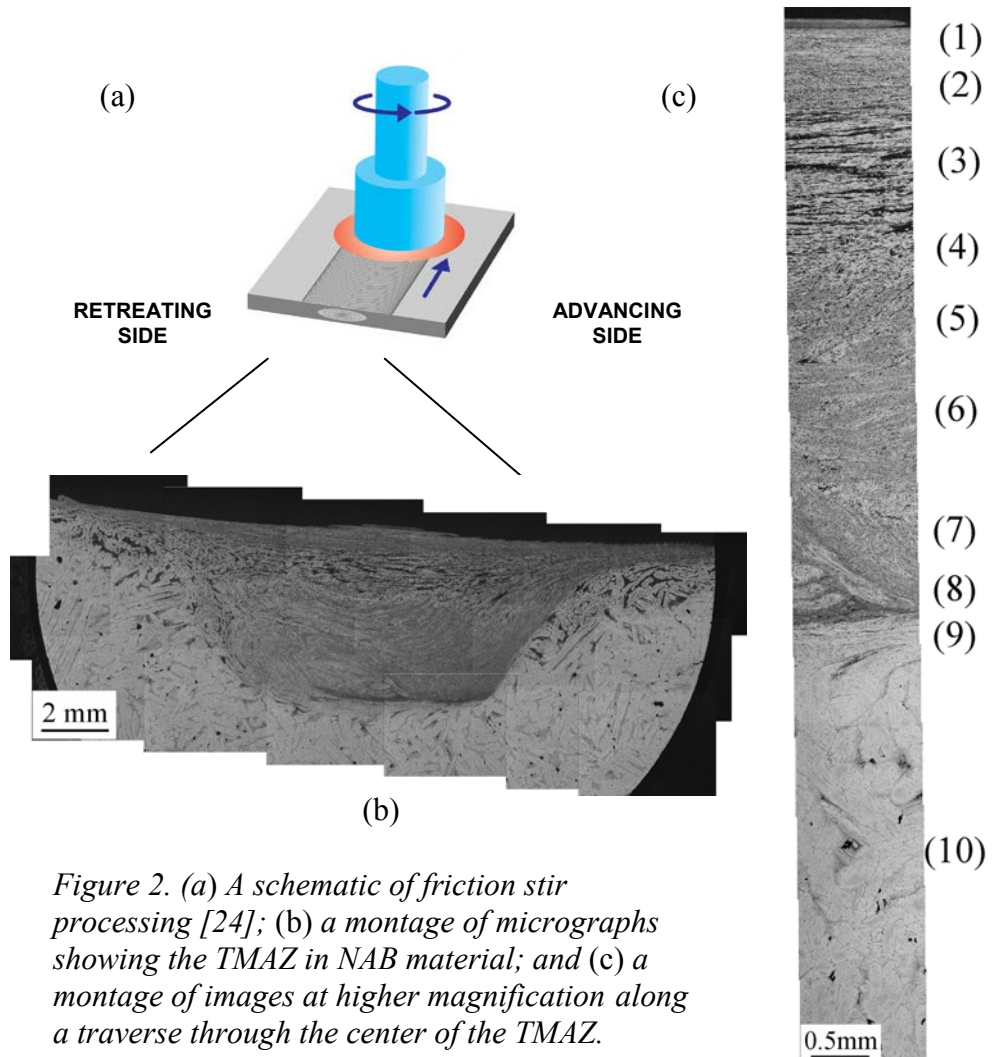

Figure 2. (a) A schematic of friction stir processing [24]; (b) a montage of micrographs showing the TMAZ in NAB material; and (c) a montage of images at higher magnification along a traverse through the center of the TMAZ.

sense of the shearing varies from location to location along the boundary. Fig. 2c is a montage of optical micrographs along a vertical traverse through the center of the TMAZ and into base metal. Region 1 near the surface exhibits a fine-grained microstructure, which is shown in Fig 3a at higher magnification. In region 3 a band-like structure is apparent; this consists of α (white areas), and martensite containing Widmanstätten α (dark areas), as shown in Fig. 3a (region 3) and, at higher magnifcation, in Fig. 3b. The decomposition of β to form Widmanstäten α and β' occurs at moderate cooling rates (Fig. 3b). These structures are elongated in a horizontal direction (perpendicular to the tool rotation axis). In the TMAZ the globular κ_{ii} precipitate particles are finer in size when compared to the κ_{ii} in as-cast material (compare Fig. 1c and Fig. 3a), and the lamellar structure of α and κ_{iii} is no longer apparent. The micrograph of region 5 is at the middle of the FSP zone and shows a highly refined and equiaxed grain size even when compared to region 1. Region 8 is directly under the tool and shows grain flow at the TMAZ / base metal boundary. The apparent grain size in this region is the finest in the TMAZ.

β

↓

Wid. α + β'

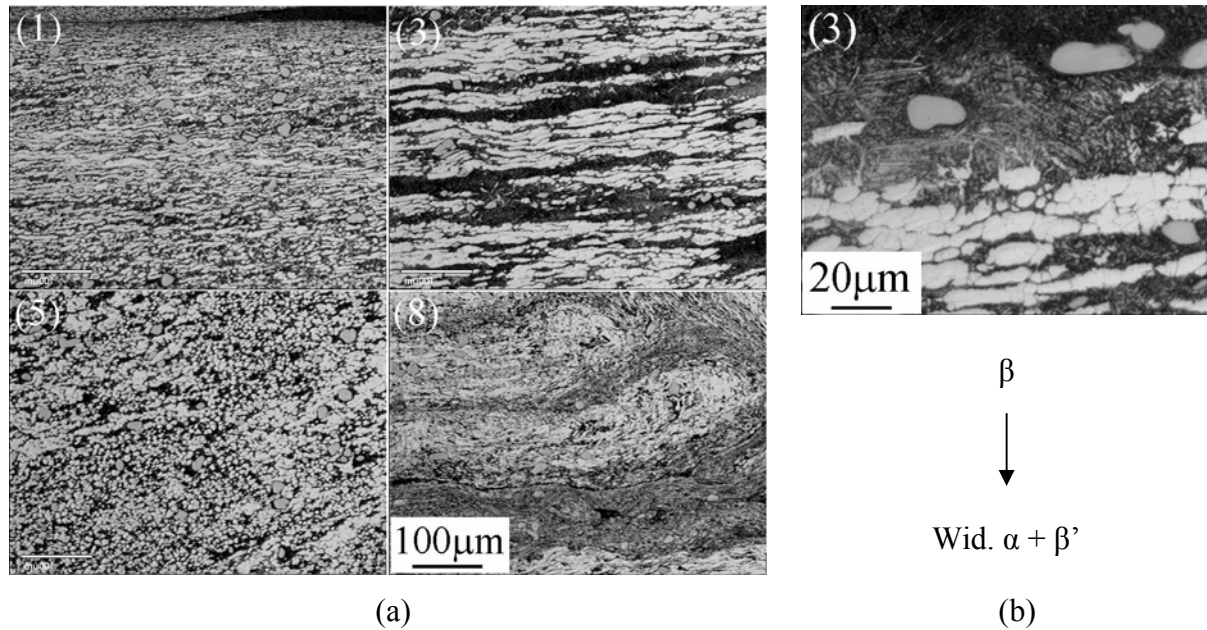(a)   (b)

Figure 3. (a) Optical micrographs from regions (1), (3), (5) and (8) at higher magnification than in Fig. 2, illustrating different microstructures from the surface downward through the TMAZ; (b) the microstructure in region (3) at still higher magnification, resolving the dark areas into Widmanstäten α and β'(martensite), suggesting that local peak temperatures were ≥ 950°C.

Results of OIM analysis for two of these regions are included in Fig. 4. as image quality maps and discrete pole figures. In the fine-grain region 8 (Fig. 4a), the image quality map suggests that the grain size is ≤ 5 μm. A random texture is apparent in the discrete pole figures, which is consistent with particle-stimulated nucleation of recrystallization in the α matrix due to the presence of the dispersed κ phases [25,26]. A single lattice orientation is observed in region 9 (Fig. 4b), which is in base metal at the TMAZ boundary. This orientation corresponds closely to a C-type shear texture component [27]; the lattice orientation and pole figures for such an orientation have been aligned with the plane of the sample in Fig. 4c. The shear direction and trace of the shear plane at this location are both aligned with the tool axis. In general, the shear plane and shear direction do not align with the TMAZ / base metal interface in this Cu – base alloy in contrast to results for Al – base materials [e.g., 23].

Results of TEM from the middle of the TMAZ (region 5) are shown in Fig. 5. Both globular and lamellar precipitate morphologies are observed. Energy dispersive analysis showed that the globular precipitates are Fe_3Al containing a small amount of Ni, and are thus κ_{ii} or κ_{iv}. The lamellar particles contain equal amounts of Fe and Ni, i.e., they are (Ni,Fe)Al, or κ_{iii}. Lamella spacing is
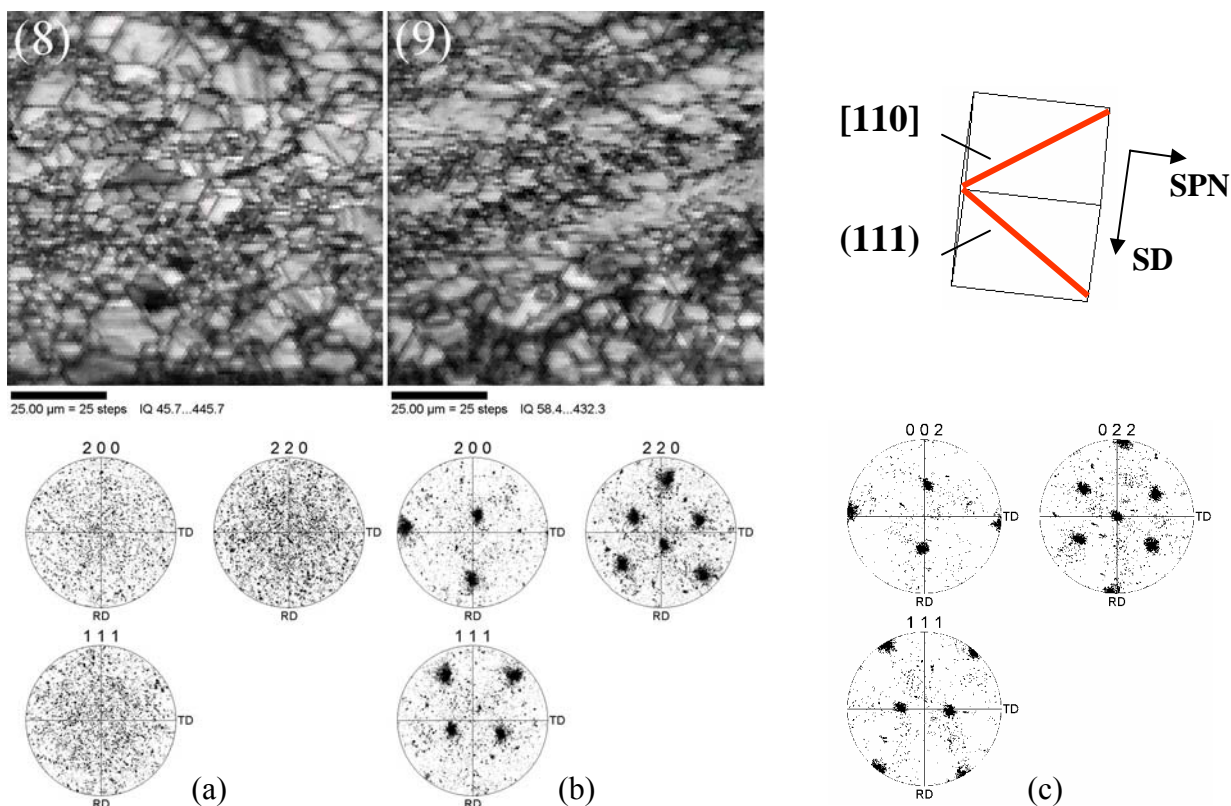
Figure 4. (a) Image quality map and discrete pole figure data for region 8, showing fine grains and a random recrystallization texture; (b) data for region 9 (just outside the TMAZ / base metal boundary) showing single lattice orientation corresponding to a C-type shear texture; (c) the C-type shear texture [27].
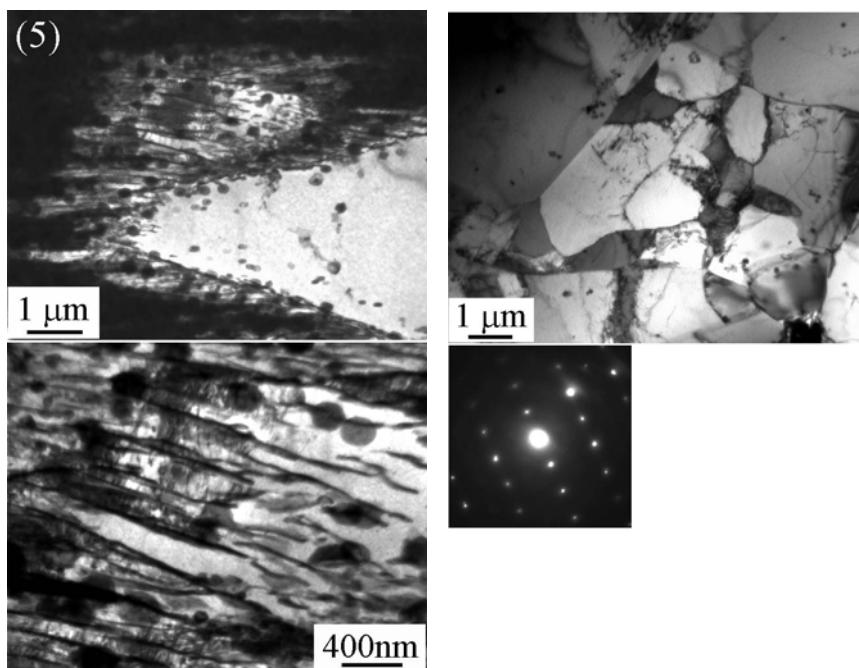

Figure 5. Transmission electron micrographs obtained from the center of the TMAZ (region 5), illustrating a grain size of about 5µm; both globular (Fe rich) and lamellar (containing both Fe and Ni) precipitates are evident

much finer than in as-cast material, which is consistent with high cooling rates and eutectoid transformation at a relatively low temperature. A subgrain structure was apparent in a nearby location within the same region suggesting that recovery and recrystallization accompany phase transformations during FSP.

The variation of microstructure in the TMAZ is consistent with severe strains, high peak temperatures, and pronounced strain, strain rate and temperature gradients. Near the surface, material has been heated to $\geq 950ºC$ so that the α and κ phases revert to β. High cooling rates near the surface result in a fine grain structure. Below the surface,

peak temperatures are lower but still sufficient for β to form and transform the Widmanstäten α and martensite on cooling. Still further beneath the surface, fine, lamellar α + κ_{iii} structures may also form.

References
[1] J.A. Duma: Naval Engineers Journal, vol. 87 (1975), p. 45
[2] R.J. Ferrara and T.E. Caton: Materials Performance, vol. 21, no. 2 (1982), p. 30
[3] R.S. Mishra and M.W. Mahoney: *Superplasticity in Advanced Materials – ICSAM 2000*, Materials Science Forum, vol. 357-9, p. 501 (Trans Tech Publications, Switzerland, 2001)
[4] P.B. Berbon, W.H. Bingel R.S. Mishra, C.C. Bampton and M.W. Mahoney: Scripta Mat., vol. 44 (2001), p. 61
[5] R.S. Mishra, M.W. Mahoney, S.X. McFadden, N.A. Mara and A.K. Mukherjee: Scripta Mat., vol. 42 (2000), p. 163
[6] M. Hansen and K. Anderenko: *Constitution of Binary Alloys* (McGraw-Hill, New York, 1958)
[7] E.A. Culpan and G. Rose: British Corrosion J, vol. 14 (1979), p. 160
[8] E.A. Culpan and G. Rose: J. Mat Sci., vol. 13 (1978), p. 1647
[9] G.M. Weston: *Survey of Nickel-Aluminum Bronze Casting Alloys for Marine Applications*, (Australia Department of Defence Report DSTO MRL-R807, Melbourne, 1981)
[10] P. Brezina: Int. Met. Rev., vol27 (1982), p. 77
[11] Metals Hanbook, 9th Ed., vol. 2
[12] G.W. Lorimer, F. Hasan, J. Iqbal and N. Ridley: British Corrosion J., vol. 21 (1986), p. 244
[13] D.M. Lloyd, G.W. Lorimer and N. Ridley: Metals Technology, vol. 7 ((1980), p. 114
[14] F. Hasan, G.W. Lorimer and N. Ridley: *Proc. Intl. Conf. On Solid to Solid Phase Transformations*, p. 745 (TMS, Warrendale, PA, 1982)
[15] F. Hasan, A. Jahanafrooz, G.W. Lorimer and N. Ridley: Metall. Trans. A, vol. 13A (1982), p. 1337
[16] F. Hasan, G.W. Lorimer and N. Ridley: Journal de Physique, vol. 43 (1982), p. C4 653
[17] A. Jahanafrooz, F. Hasan, G.W. Lorimer and N. Ridley: Metall. Trans. A, vol. 14A (1983), p. 1951
[18] F. Hasan, G.W. Lorimer and N. Ridley: Metal Sci., vol. 17 (1983), p. 289
[19] F. Hasan, J. Iqbal and N. Ridley: Mater. Sci. and Tech., vol. 1 (1985), p. 312
[20] P. Weill-Couly and D. Arnaud: Fonderie, no. 322 (1973), p. 123
[21] K.V. Jata and S.L. Semiatin: Scripta Mat., vol. 43 (2000), p. 743
[22] G. Liu, L.E. Murr, C.S. Niou, J.C. McClure and F.R. Vega: Scripta Mat., vol. 37 (1997), p.355
[23] D.P. Field, T.W. Nelson, Y. Hovanski and K.V. Jata: Metall. and Mater. Trans. A, vol. 32A (2001), p. 2869
[24] M.W. Mahoney, Rockwell Scientific Company, Thousand Oaks, CA, Private Communication, December, 2002
[25] F.J. Humphreys: Acta Metall., vol. 25 (1977), p. 1323
[26] R.D. Doherty, D.A. Hughes, F.J. Humphreys, J.J. Jonas, D. Juul-Jensen, M.E. Kassner, W.E. King, T.R. McNelley, H.J. McQueen and A.D. Rollett: Mater. Sci. Eng. A, vol. A238 (1987), p. 219
[27] G.R. Canova, U.F. Kocks and J.J. Jonas: Acta Metall., vol. 32 (1984), p. 211